

## Crystal structure and iron topochemistry of erionite-K from Rome, Oregon, U.S.A.

PAOLO BALLIRANO,<sup>1,2</sup> GIOVANNI B. ANDREOZZI,<sup>1,3</sup> MERAL DOGAN,<sup>4</sup> AND A. UMRAN DOGAN<sup>5,6,\*</sup>

<sup>1</sup>Dipartimento di Scienze della Terra, Sapienza Università di Roma, P.le A. Moro, 5, I-00185 Rome, Italy

<sup>2</sup>CNR-IGAG, Istituto di Geologia Ambientale e Geoingegneria, Sede di Roma, Via Bolognola 7, I-00138 Rome, Italy

<sup>3</sup>CNR-IGG, Istituto di Geoscienze e Georisorse, Sede di Roma, P.le A. Moro, 5, I-00185 Rome, Italy

<sup>4</sup>Department of Geological Engineering, Hacettepe University, Ankara, Turkey

<sup>5</sup>Department of Geological Engineering, Ankara University, Ankara, Turkey

<sup>6</sup>Department of Chemical and Biochemical Engineering, The University of Iowa, Iowa City, Iowa 52242, U.S.A.

### ABSTRACT

A complete crystal-chemical characterization of erionite-K from Rome, Oregon, was obtained by combining field emission scanning electron microscopy, laboratory parallel-beam transmission powder diffraction, and <sup>57</sup>Fe Mössbauer spectroscopy. Rietveld refinement results evidenced that the most striking difference in comparison with the structure of erionite-Ca is significant K at a K2 site ( $\frac{1}{2}$ , 0, 0), which is empty in erionite-Ca. In addition, site Ca1 shows low occupancy and Ca3 is vacant. The oxidation and coordination state of Fe, whose occurrence was revealed by chemical analysis, have been clarified by exploiting room- and low-temperature <sup>57</sup>Fe Mössbauer spectroscopy. The majority of Fe (95%) was attributed to Fe<sup>3+</sup>-bearing, superparamagnetic, oxide-like nanoparticles with dimensions between 1 and 9 nm, and the remaining 5% was attributed to hematite particles with size  $\geq 10$  nm, both located on the crystal surface.

**Keywords:** Oregon erionite, erionite-K, crystal structure, iron topochemistry, field emission, scanning electron microscopy, laboratory parallel-beam transmission powder diffraction, Rietveld refinement, <sup>57</sup>Fe Mössbauer spectroscopy

### INTRODUCTION

Erionite (ERI) is a fibrous zeolite-group mineral, often occurring as altered products of volcanic ash. From the structural point of view, it belongs to the ABC-6 family (Gottardi and Galli 1985), and its framework consists of columns of cancrinite ( $\epsilon$ ) cages connected along the  $z$  direction by double 6-rings (D6R) (Staples and Gard 1959). Erionite cages (23-hedra) are formed by linking adjacent columns via single 6-rings (S6R) at the level of  $\epsilon$ -cages (Fig. 1). The erionite framework can also be described by the stacking along the  $z$  direction of 6-rings following the AABAAC sequence. Intergrowth of erionite with offretite (OFF) may occur, due to the close similarity between the two zeolites. In fact, offretite has an AABAAB sequence, and stacking faults corresponding to partial substitution of C with B 6-rings have been observed (Schlenker et al. 1977). Erionite is hexagonal, space group  $P6_3/mmc$  (Kawahara and Curien 1969) and has an average formula  $K_2(\text{Na}, \text{Ca}_{0.5})_8[\text{Al}_{10}\text{Si}_{26}\text{O}_{72}] \cdot 30\text{H}_2\text{O}$  (Coombs et al. 1997). A large chemical variability is typical of this mineral, and for this reason three different species are identified, according to the most abundant extra-framework cation: erionite-Na, erionite-K, and erionite-Ca (Coombs et al. 1997; Passaglia et al. 1998; Gualtieri et al. 1998; Dogan and Dogan 2008).

Erionite is a nominally Fe-free phase, but in several cases a Fe<sub>2</sub>O<sub>3</sub> content up to 3 wt% has been observed (Eberly 1964; Dogan et al. 2006). This point should be further explored, since Dogan et al. (2006) reported a comparison between erionite

from Rome, Oregon, and erionite from the Cappadocia region, Turkey, the latter being responsible for the malignant mesothelioma epidemic. All analyzed samples showed significant Fe contents. Erionite from Rome, Oregon, seems to have a content of Fe<sub>2</sub>O<sub>3</sub> even higher than the Cappadocia erionite, but occurs in a region where, thus far, it has not been associated with malignant mesothelioma.

The Fe presence/absence, as well as its content, oxidation, and coordination state, and behavior, are of particular relevance. In fact, it is well known from amphibole asbestos that Fe has been

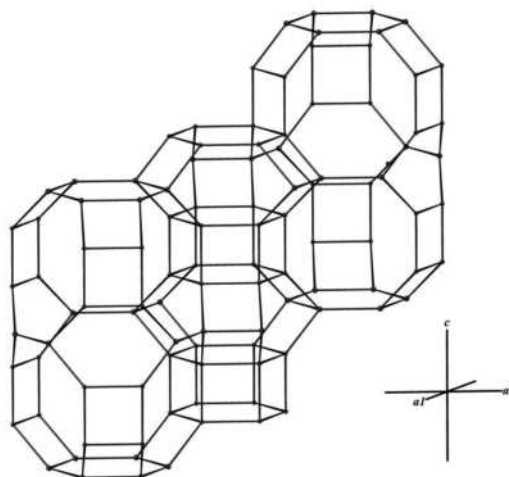


FIGURE 1. Framework of erionite (Atoms 5.1: Dowty 2000).

\* E-mail: umran-dogan@uiowa.edu

claimed to be one of the causes of carcinogenesis by participating in Fenton chemistry and producing free radicals (e.g., Kane et al. 1996; Fubini and Otero Aréan 1999; Kamp and Weitzman 1999; Robledo and Mossman 1999). Similarly, erionite toxicity was ascribed to ion-exchanged and/or surface-deposited Fe that participates in Fenton chemistry (Eborn and Aust 1995). Moreover, it was proposed that even upon inhalation of Fe-free fibers, they can imbibe Fe via ion-exchange because protein injury can lead to metal ion release (Carr and Frei 1999). In any case, whether Fe is carried on from erionite or is captured in the lungs, it was highlighted that the Fenton chemistry occurs on the surface of the fibers and that the coordination state of Fe is critical for inducing cytotoxicity and genotoxic damage (Fach et al. 2003; Ruda and Dutta 2005). Moreover, the molecular mechanisms by which mineral fibers induce genotoxic damage remain unclear (or poorly understood so far), since the appearance of malignant mesothelioma in humans has been found to be also dependent on genetic predisposition (Dogan et al. 2006, 2008; Bertino et al. 2007; Carbone et al. 2007).

Morphostructural/biological activity relationships in erionite is a crucial subject still to be clarified, and a detailed crystal-chemical investigation would be a fundamental first step. The present work reports new data on the crystal chemistry of erionite-K from Rome, Oregon, from combined field emission scanning electron microscopy (FESEM),  $^{57}\text{Fe}$  Mössbauer spectroscopy (MS), and laboratory parallel-beam transmission powder X-ray diffraction data (PXRD).

## EXPERIMENTAL METHODS

### Field emission scanning electron microscopy

Field emission scanning electron microscopy images were obtained with a Hitachi S-4800 SEM with an accelerating voltage of 5 kV. Very small (ca.  $5 \times 5 \times 30 \mu\text{m}$ ), well-developed, prismatic crystals were observed (Fig. 2a). They consist of the  $\{10\bar{1}0\}$  (hexagonal prism) and  $\{0001\}$  (pinacoid) forms. However, the prevailing morphology is that of very thin fibrils arranged to form fibers and bundles up to  $50 \mu\text{m}$  of length. The diameter of individual fibrils forming the erionite bundles is of the order of  $0.5 \mu\text{m}$  or less (Fig. 2b). No clear evidence of any crystalline phase other than erionite was observed.

### $^{57}\text{Fe}$ Mössbauer spectroscopy

The fibers of erionite were gently ground in an agate mortar with acetone and mixed with a powdered acrylic resin to avoid preferred orientations. Since Fe total content was expected to be not larger than 4 wt% (Dogan et al. 2006), about 100 mg of sample was used, so that the absorber was within the limits for the thin absorber thickness described by Long et al. (1983). Absorption spectra were collected at both room temperature (RT) (Fig. 3a) and 77 K (Fig. 3b) in a liquid nitrogen cryostat, using a conventional spectrometer system operated in constant acceleration mode with a  $^{57}\text{Co}$  source of nominal strength of 25 mCi in an Rh matrix. Data were recorded in a multichannel analyzer using 512 channels for the velocity range  $-10$  to  $10 \text{ mm/s}$ . To have good statistics, up to 10 million counts per channel were collected. After velocity calibration against a spectrum of high-purity  $\alpha$ -iron foil ( $25 \mu\text{m}$  thick), the raw data were folded to 256 channels. The spectra were fitted using the Recoil 1.04 fitting program (Lagarec and Rancourt 1998). A first cycle was done fitting pure Lorentzian line shapes, and results were quite satisfying ( $\chi^2 < 1$  and linewidths up to  $0.50 \text{ mm/s}$ ). In spite of this, a second refining cycle was performed fitting quadrupole splitting distributions (QSD), following the successful approach of Rancourt and Ping (1991) and Rancourt (1994a, 1994b). Several fitting models with unconstrained parameters were tried to get a best fit. Results of both the Lorentzian and the QSD approach were in agreement and this gave a good confidence in the physical correctness of the distribution analysis. Uncertainties were calculated using the covariance matrix and errors were estimated to be approximately  $\pm 5\%$  for absorption areas (Table 1).

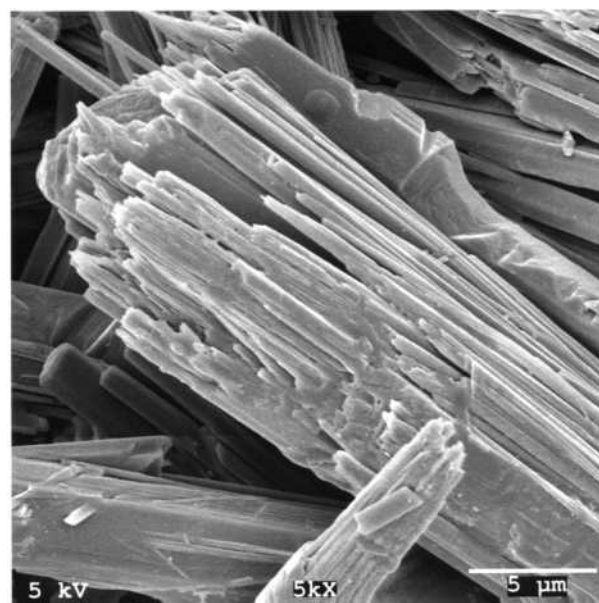
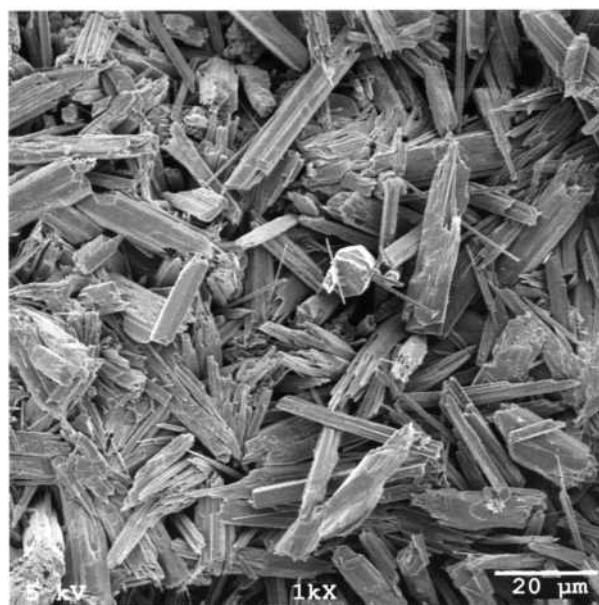


**FIGURE 2.** (a) Field emission scanning electron images of erionite-K from Rome, Oregon, showing well-developed prismatic crystals. Accelerating voltage = 5 kV, bar scale =  $20 \mu\text{m}$ . (b) Close-up FESEM image of erionite-K showing very thin fibrils arranged to form fibers and bundles. Accelerating voltage = 5 kV, bar scale =  $5 \mu\text{m}$ .

### Powder X-ray diffraction

A preliminary fast scan excluded the presence of impurities at the 0.5 wt% level (determined by analyzing synthetic erionite/quartz mixtures at different dilutions). The powder of erionite was loaded in a  $0.7 \text{ mm}$  diameter  $\text{SiO}_2$ -glass capillary that was subsequently aligned on a standard goniometer head. Data were collected on a parallel-beam Bruker AXS D8 Advance automated diffractometer operating in  $\theta$ - $\theta$  geometry. It is fitted with an incident-beam Göbel mirror, diffracted-beam radial Soller slits, and a PSD VANTEC-1 detector. Diffraction data were collected in the angular range  $5$ – $140^\circ 2\theta$ , with a step-size of  $0.0214^\circ 2\theta$ , using  $\text{CuK}\alpha$  radiation and were evaluated by the Rietveld method using the GSAS crystallographic suite of programs (Larson and Von Dreele 1985) coupled to the EXPGUI graphical user interface (Toby 2001). The background was fitted with a 36-term Chebyshev polynomial of the first kind to model the

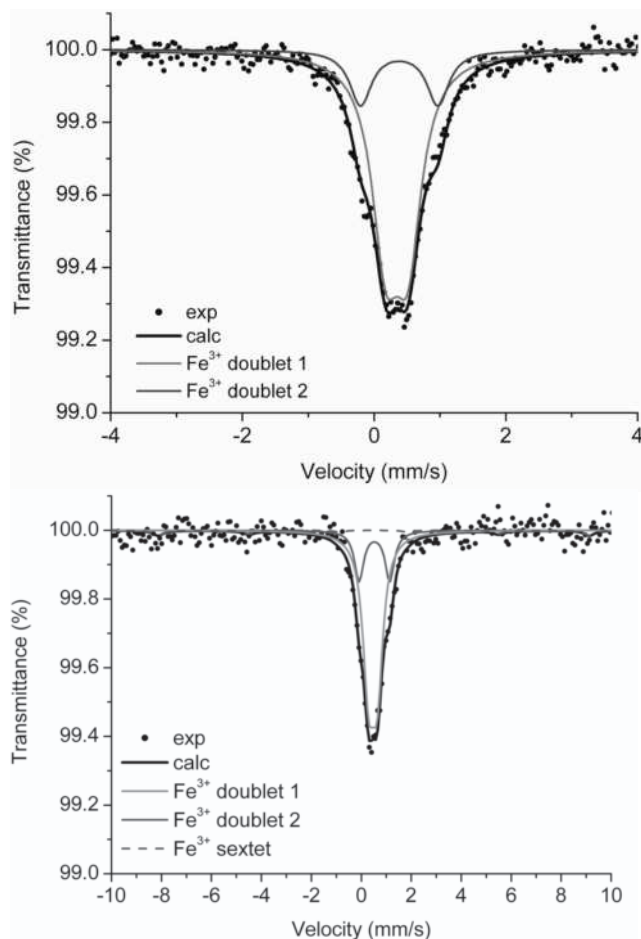


**FIGURE 3.**  $^{57}\text{Fe}$  Mössbauer spectra of erionite-K from Rome, Oregon, collected at: (a) room temperature, from  $-4$  to  $4$  mm/s; (b)  $77$  K, from  $-10$  to  $10$  mm/s.

amorphous contribution arising from the capillary. Peak-shapes were fitted by the TCH (Thompson, Cox, Hastings) pseudo-Voigt function (Thompson et al. 1987), modified for asymmetry (Finger et al. 1994). Refined variables were GV and GW (tan  $\theta$ -dependent and angle-independent, respectively) Gaussian parameters, LX and LY ( $1/\cos \theta$ - and tan  $\theta$ -dependent) Lorentzian parameters, and S/L and H/L asymmetry parameters (constrained to be equal in magnitude). Peak positions were corrected for sample displacement from the focusing circle. An absorption parameter was refined. Starting structural parameters were those of Alberti et al. (1997) consisting, apart from the framework, of four cationic sites [K (hereafter renamed as K1), Ca1, Ca2, and Ca3] and six  $\text{H}_2\text{O}$ -molecules sites (OW7, OW8, OW9, OW10, OW11, and OW12). Immediately Ca3 site occupancy reduced to zero and, for this reason, the site was removed from the refinement. Difference Fourier maps calculated from the refined model located a further cationic site at special position  $\frac{1}{2}, 0, 0$  corresponding to the K site reported by Schlenker et al. (1977) for dehydrated erionite and hereafter labeled K2. Bond distances and angles were completely unrestrained. Displacement parameters for K1 and K2, Ca1 and Ca2, and OW8, OW9, OW10, OW11, and OW12 were constrained to be equal in magnitude (Ow7 unconstrained as lying on  $mm2$ ). However, after a few cycles of refinement the  $U_{\text{iso}}$  isotropic displacement parameter of OW7 was set and kept fixed to the value of  $0.08 \text{ \AA}^2$  reported by Alberti et al. (1997), because of strong correlation with the corresponding site occupancy. Site populations for all cationic and  $\text{H}_2\text{O}$ -molecules sites were refined. Attempts to model the presence of preferred orientation by means of the generalized spherical harmonics description of Von Dreele (1997) produced a small improvement of the fit as a result of a J texture index of 1.105. Convergence was reached at  $R_p = 2.64\%$ ,  $R_{wp} = 3.31\%$ ,  $R_{f2} = 4.31\%$ , and reduced  $\chi^2 = 4.52$ . At this point the structural data were used and recycled in a further refinement using TOPAS v. 3.0 (Bruker AXS 2005). This program implements the Fundamental Parameters Approach FPA (Cheary and Coelho 1992) and is claimed to be able to provide a more accurate description of the peak-shape. In

**TABLE 1.** Mössbauer parameters and site attribution for erionite-K from Rome, Oregon

T (K)	$\chi^2$	IS (mm/s)	QS (mm/s)	W (mm/s)	Area (%)	Iron species— Site attribution
298	0.89	0.34	0.34	0.50	80	$\text{Fe}^{3+}$ (octahedral)
		0.38	1.17	0.40	20	$\text{Fe}^{3+}$ (octahedral)
77*	0.51	0.46	0.35	0.54	73	$\text{Fe}^{3+}$ (octahedral)
		0.52	1.23	0.44	22	$\text{Fe}^{3+}$ (octahedral)

Note: IS = isomer shift (with respect to  $\alpha$ -iron); QS = quadrupole splitting; W = linewidth at half maximum; estimated uncertainties =  $0.05$  mm/s for all parameters and 5% absolute for the area.

\*A weak magnetic sextet is included, with IS =  $0.5$ , magnetic field  $H = 54$  T, and area =  $5$ .

fact, keeping the same constraints on displacement parameters, we were able to significantly reduce the agreement indices to  $R_p = 1.93\%$ ,  $R_{wp} = 2.60\%$ ,  $R_{\text{Bragg}} = 0.80\%$ , and reduced  $\chi^2 = 3.54$ . No significant structural differences were observed between the two refinements. Experimental details and miscellaneous data of the latter refinement are reported in Table 2, positional and displacement parameters of non-hydrogen atoms in Table 3, relevant bond distances and angles in Table 4, bond valences (according to Brese and O'Keefe 1991) in Table 5, and experimental, calculated, and difference plots in Figure 4.

## RESULTS

### Chemical composition

The chemical composition of erionite-K from Rome, Oregon, was reported by Eberly (1964) and Dogan et al. (2006). A difference in  $\text{K}_2\text{O}$  and in  $\text{H}_2\text{O}$  contents may be observed (Table 6), but the crystal chemical formula based on the second one is more accurate—because the oxides were not measured for Sample 1—and close to erionite stoichiometry  $\text{K}_2(\text{Na}, \text{Ca}_{0.5})_8(\text{Al}_{10}\text{Si}_{26}\text{O}_{72}) \cdot 30\text{H}_2\text{O}$ .

However, the water content measured by Dogan et al. (2006) appeared to be anomalously low (13 wt%), therefore it was re-examined here. A thermogravimetric analysis was carried out on 16 mg of sample using a Netzsch STA 409 PC Luxx TG/DTA, operating in air, using a heating rate of  $5$  K/min. A total weight loss of 16.0 wt% was measured. In spite of this, even with the new water content, the calculated oxygen in the crystal chemical formula significantly exceeded 72 atoms per formula unit (apfu). However, after removal of  $\text{TiO}_2$  and  $\text{Fe}_2\text{O}_3$  from the

**TABLE 2.** Experimental details of powder X-ray diffraction data collection and miscellaneous data of the Rietveld refinement

Instrument	Bruker AXS D8 Advance
X-ray tube	Cu at 40 kV and 40 mA
Incident beam optic	Multilayer X-ray mirrors
Sample mount	Rotating capillary (60 rpm)
Soller slits	2 ( $2.3^\circ$ divergence + radial)
Divergence slit	0.1 mm
Detector	PSD VÅntec-1
Detector window	$6^\circ$
$2\theta$ range ( $^\circ$ )	5–140 (6325 data points)
Step size ( $^\circ$ )	0.0214
Counting time (s)	30
Space group	$P6_3/mmc$
$a$ ( $\text{\AA}$ )	13.22794(9)
$c$ ( $\text{\AA}$ )	15.06946(10)
$V$ ( $\text{\AA}^3$ )	2283.56(3)
$R_{\text{Bragg}}$ (%)	0.80
$R_p$	1.93
$wR_p$	2.60
$\chi^2$	3.54
$L_{\text{vol}}$ (nm)	103.7(19)
$\epsilon_0$	0.0479(14)

Notes: Statistical parameters as defined in Young (1993).  $L_{\text{vol}}$  defined as  $\beta_1 = \lambda/L_{\text{vol}} \cos \theta$ ;  $\epsilon_0$  defined as  $\beta_1 = 4\epsilon_0 \tan \theta$ .

**TABLE 3.** Fractional coordinates, isotropic displacement parameters, site multiplicity and occupancy, and site scattering of erionite-K

Site	x	y	z	Site mult.	Site occ.	$U_{iso}$ (Å <sup>2</sup> )	s.s. (e <sup>-</sup> )	Proposed site partition	s.s. (e <sup>-</sup> ) from site partition
Framework									
Si1	0.23397(12)	-0.00016(16)	0.10440(6)	24	1	0.0054(3)		Si <sub>20.56</sub> + Al <sub>3.44</sub>	
Si2	0.09314(18)	0.42355(18)	¼	12	1	0.0091(5)		Si <sub>8.67</sub> + Al <sub>3.33</sub>	
O1	0.34747(22)	0.02431(20)	0.66096(19)	24	1	0.0122(9)			
O2	0.09799(15)	0.1960(3)	0.12546(23)	12	1	0.0108(15)			
O3	0.12540(15)	0.2508(3)	0.6335(3)	12	1	0.0242(15)			
O4	0.26678(22)	0	0	12	1	0.0125(12)			
O5	0.23430(25)	0.4686(5)	¼	6	1	0.0318(23)			
O6	0.45910(25)	0.9182(5)	¼	6	1	0.0339(23)			
Extraframework cations									
K1	0	0	¼	2	0.976(5)	0.0286(15)*	37.1(2)	K <sub>2.00</sub>	38.0
K2	½	0	0	6	0.135(5)	0.0286(15)*	15.4(5)	K <sub>0.87</sub>	16.5
Ca1	0.308(5)	0.617(10)	0.872(4)	12	0.093(15)	0.202(12)†	13(2)	Mg <sub>0.80</sub>	9.6
Ca2	0.3065(8)	0.6130(16)	0.0902(7)	12	0.301(5)#	0.202(12)†	39.7(7)	Na <sub>2.00</sub> + Ca <sub>0.86</sub> + Mn <sub>0.02</sub>	39.7
						$\Sigma_{cat}$	105.2		103.8
Water molecules									
OW7	0.2299(6)	0.4597(12)	¾	6	0.744(21)	0.080‡	35.7(10)		
OW8	0.2635(11)	0.5269(21)	-0.0388(19)	12	0.279(7)	0.182(5)§	26.8(7)		
OW9	0.4317(10)	0.8633(21)	0.921(3)	12	0.377(14)	0.182(5)§	36.2(13)		
OW10	0.4352(7)	0.8704(14)	0.6626(16)	12	0.458(16)	0.182(5)§	44.0(15)		
OW11	0.2667(18)	0.533(4)	0.681(3)	12	0.366(15)	0.182(5)§	35.1(14)		
OW12	0.4435(6)	0.8871(11)	0.0143(9)	12	0.693(13)	0.182(5)§	66.5(12)		
						$\Sigma_{water}$	244.3		

Note: Si/Al partition from Jones' (1968) determinative curves.

\* Constrained to be equal.

† Constrained to be equal.

‡ Unrefined.

§ Constrained to be equal.

|| Scattering power of Mg.

# Scattering power of Na.

**TABLE 4.** Relevant bond distances (Å) and angles (°) of erionite-K from Rome, Oregon; non-occurring distances are in *italic*

Si1-O1	1.612(3)		O1-Si1-O2	111.40(16)
Si1-O3	1.6221(14)		O1-Si1-O3	108.69(15)
Si1-O4	1.6317(13)		O1-Si1-O4	106.84(13)
Si1-O2	1.6381(11)		O2-Si1-O3	106.89(17)
<Si1-O>	1.626		O2-Si1-O4	111.98(13)
			O3-Si1-O4	111.04(13)
Si2-O6	1.633(3)		O1-Si2-O1	108.72(19)
Si2-O1 ×2	1.651(3)		O1-Si2-O5 ×2	113.53(13)
Si2-O5	1.652(3)		O1-Si2-O6 ×2	107.14(19)
<Si2-O>	1.647		O5-Si2-O6	106.4(3)
Si1-O1-Si2	142.11(22)		Si1-O4-Si1	149.23(23)
Si1-O2-Si1	141.47(25)		Si2-O5-Si2	143.6(4)
Si1-O3-Si1	145.6(3)		Si2-O6-Si2	170.87(13)
K1-O2 ×6	2.926(3)	K		
K1-O3 ×6	3.367(3)	K		
K2-OW12 ×2	1.311(13)			
K2-OW9 ×2	1.97(3)			
K2-OW10 ×2	2.865(22)	K		
K2-O4 ×2	3.085(3)	K		
K2-O1 ×4	3.272(3)	K		
K2-OW8 ×4	3.37(2)	K		
Ca1-OW11	1.25(11)			
Ca1-OW8	1.69(9)			
Ca1-OW11 ×2	2.05(11)	Mg		
Ca1-OW9 ×2	2.16(5)	Mg		
Ca1-OW10 ×2	2.17(4)			
Ca1-OW8 ×2	2.37(8)	Mg		
Ca1-OW7	2.57(9)			
Ca1-OW9	2.92(12)			
Ca1-OW10	2.95(12)			
Ca1-OW11	3.03(8)			
Ca1-OW12 ×2	3.14(3)			
Ca1-OW7 ×2	3.27(4)			
Ca2-OW8	2.18(3)	Ca Na		
Ca2-OW12 ×2	2.552(15)	Ca Na		
Ca2-OW8 ×2	2.77(3)	Ca Na		
Ca2-O5	2.922(14)	Ca Na		
Ca2-OW9 ×2	3.25(3)			
Ca2-OW12	3.342(15)	Ca Na		

Note: K, Na, Ca, and Mg symbols refer to possible cationic coordination.

**TABLE 5.** Bond valence analysis (v.u.) following Breese and O'Keeffe (1991)

	K	Na	Mg	Ca
K1-O2 ×6	0.116 ×6			
K1-O3 ×6	0.035 ×6			
$\Sigma$	0.906			
K2-OW10 ×2	0.137 ×2			
K2-O4 ×2	0.076 ×2			
K2-O1 ×4	0.046 ×4			
K2-O8 ×4	0.035 ×4			
$\Sigma$	0.750			
Ca1-OW11 ×2			0.381 ×2	
Ca1-OW9 ×2			0.283 ×2	
Ca1-OW8 ×2			0.161 ×2	
$\Sigma$			1.650	
Ca2-OW8		0.358		0.562
Ca2-OW12 ×2		0.131 ×2		0.206 ×2
Ca2-OW8 ×2		0.073 ×2		0.114 ×2
Ca2-O5		0.048		0.076
Ca2-OW12		0.016		0.024
$\Sigma$		0.830		1.302

total (attributed to impurity, following the assignment of Eberly (1964) and on the basis of structural and spectroscopic evidence) and normalizing to 100%, the corresponding chemical formula of the present sample became:  $K_{2.87}Na_{2.00}Ca_{0.86}Mg_{0.80}Mn_{0.02}(Al_{6.95}Si_{29.05}O_{72.64}) \cdot 25.66H_2O$ .

It is worth noting that, from comparison of the Mössbauer absorption spectra collected on the erionite-K from Rome, Oregon, with those collected on synthetic, microporous zeolites (with known Fe content), the average Fe content of our sample should not be higher than 1 wt%. Many attempts to quantify Fe content of other erionite samples (Dogan and Dogan 2008) gave values very different from point to point, supporting in this way the hypothesis of Fe coming from heterogeneous impurities. Passaglia et al. (1998) reported compositions of both erionite

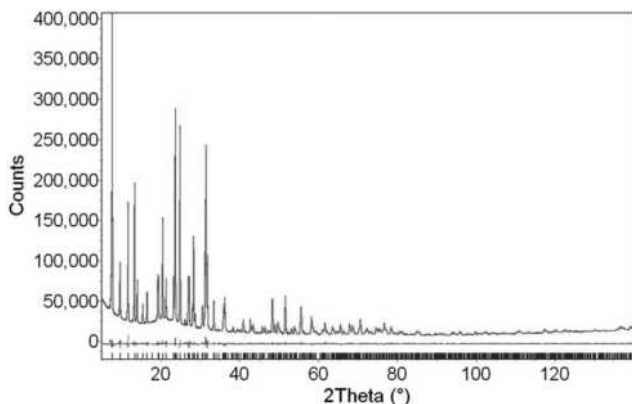


**FIGURE 4.** Experimental (dots), calculated (solid line), and difference (below) plots of the Rietveld refinement of erionite-K from Rome, Oregon. Vertical markers refer to calculated Bragg reflections.

**TABLE 6.** Reference chemical data for erionite-K from Rome, Oregon: (1) Eberly (1964); (2) Dogan et al. (2006); (3) modified from Dogan et al. (2006)

	1	2	3
SiO <sub>2</sub>	60.81	60.70	61.63
TiO <sub>2</sub>	–	0.48	–
Al <sub>2</sub> O <sub>3</sub>	13.59	12.32	12.51
Fe <sub>2</sub> O <sub>3</sub>	3.63	3.39	–
MgO	0.80	1.12	1.14
CaO	1.54	1.67	1.70
MnO	–	0.05	0.05
Na <sub>2</sub> O	1.90	2.16	2.19
K <sub>2</sub> O	7.17	4.71	4.78
P <sub>2</sub> O <sub>5</sub>	–	0.07	–
H <sub>2</sub> O	10.57	13.06	16.00*
Total	100.01	99.73	100
Si	28.49	29.05	29.05
Ti	–	0.17	–
Al	7.51	6.95	6.95
Fe	1.28	1.22	–
Mg	0.56	0.80	0.80
Ca	0.77	0.86	0.86
Mn	–	0.02	0.02
Na	1.73	2.00	2.00
K	4.29	2.88	2.87
H <sub>2</sub> O	16.52	20.85	25.66
O	74.51	74.77	72.64
R	0.791	0.807	0.807
M	6.02	4.88	4.87
D	1.33	1.68	1.68
M/(M+D)	0.82	0.75	0.74
Ca/D	0.58	0.51	0.51
Na/M	0.29	0.41	0.41

Notes: Data were recalculated after removal of oxides considered arising from contaminants. Crystal-chemical formulae normalized on the basis of 36 (Si+Al).

\* From new TGA analytical data. R = Si/(Si+Al); M = Na+K; D = ΣCa+Mg+Mn.

and offretite samples from Oregon. Figure 5 shows corresponding extra-framework cation compositions of the present erionite sample and Passaglia et al. (1998) samples.

### <sup>57</sup>Fe Mössbauer spectroscopy

Fe-containing natural and synthetic microporous materials are widely studied, especially because of their activity as catalysts in various acidic or oxidation reactions. Many different methods (diffractometric, magnetic, spectroscopic) have been used; among these, <sup>57</sup>Fe Mössbauer spectroscopy is one of the most

used because of several advantages, first of all the sensitivity to Fe oxidation and aggregation state (Meagher et al. 1988; Bachari et al. 2007). In fact, whenever Fe is present in a zeolite structure, its oxidation state (i.e., the Fe<sup>2+</sup>/Fe<sup>3+</sup> ratio) must be clarified, but this is not enough. In addition to that, its location at (1) framework sites, (i.e., tetrahedrally coordinated, substituting for Si/Al); (2) extra-framework positions (in the cages); or (3) the external surfaces should be investigated, because its aggregation state, the so-called “nuclearity”; as (4) single ion; (5) dinuclear Fe<sub>x</sub>O<sub>y</sub> cluster; or (6) Fe<sub>2</sub>O<sub>3</sub> hematite particle is of extremely high interest (Zecchina et al. 2007 and references therein). As mentioned before, for erionite both Fe location and nuclearity are very important because they would strongly affect the Fe availability and bioactivity (Fach et al. 2003; Ruda and Dutta 2005).

The <sup>57</sup>Fe Mössbauer spectrum of erionite collected at RT (Fig. 3a) shows a broad absorption signal, which was initially modeled by a close quadrupole doublet with an isomer shift (IS) of 0.34 mm/s relative to α-iron and a quadrupole splitting (QS) of 0.37 mm/s, indicating the presence of high-spin Fe<sup>3+</sup> ions. However, the large value of linewidth (0.75 mm/s) suggested the presence of at least two overlapping signals. A second model with two doublets gave better resolution, with a first doublet (80% of Fe<sub>tot</sub>) characterized by IS = 0.34 mm/s, QS = 0.34 mm/s, and linewidth of 0.50 mm/s, and a second doublet (20% of Fe<sub>tot</sub>) characterized by IS = 0.38 mm/s, QS = 1.17 mm/s, and linewidth of 0.40 mm/s. On the basis of the IS values, the two doublets may be ascribed to Fe<sup>3+</sup> octahedrally coordinated (Meagher et al. 1988). A third model was also tried, and a third doublet (5% of Fe<sub>tot</sub>) with IS = 0.16 mm/s, QS = 0.64 mm/s, and linewidth of 0.20 mm/s was refined, but the area of the third doublet showed an error larger than its value and the model was rejected.

### Structural analysis

Microstructural parameters were extracted by evaluating the integral breadths β<sub>i</sub> of the individual reflections from the X-ray diffraction data. A volume-weighted mean column height L<sub>vol</sub>,

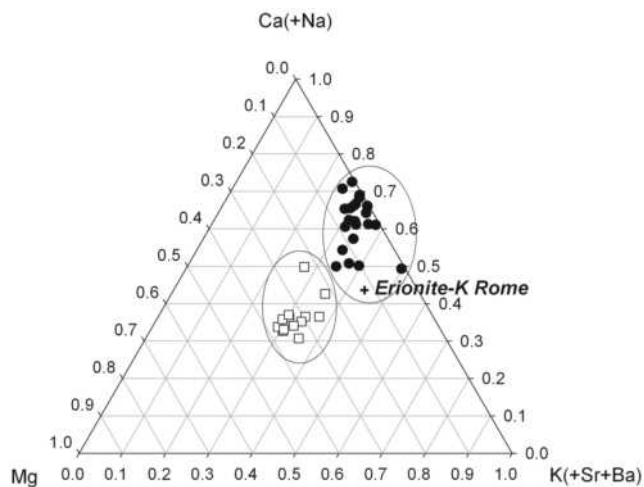


**FIGURE 5.** Compositional diagram based on the extra framework cation content of erionite (full circle) and offretite (open square) samples studied by Passaglia et al. (1998) and the corresponding composition of the present sample (cross).

defined as  $\beta_i = \lambda/L_{\text{vol}} \cos \theta$ , of 1037(19) Å was refined. Moreover, an  $\epsilon_0$  microstrain (lattice strain), defined as  $\beta_i = 4\epsilon_0 \tan \theta$ , of 0.0479(14) was obtained.

**Framework.** The two independent tetrahedral sites T1 and T2 (building, respectively the D6R and the S6R) are characterized by a disordered Si/Al distribution. In fact,  $\langle \text{T1-O} \rangle - \langle \text{T2-O} \rangle$  is  $-0.021$  Å, clearly indicating the preferential partition of Al on T2. From Jones' (1968) determinative curve a distribution of Al as 14.3% of T1 (corresponding to 3.44 apfu) and 27.8% of T2 (corresponding to 3.33 apfu) has been calculated. Therefore, a total of 6.77 Al apfu was estimated, as compared to 6.95 apfu from recalculated chemical data. However, it is well known that, in the case of a disordered Si/Al distribution, the curve of Jones provides systematically underestimated values. Moreover, according to the regression equation of Passaglia et al. (1998) [ $R = \text{Si}/(\text{Si}+\text{Al}) = 5.65149 - 0.00213 \times \text{Volume} (\text{Å}^3)$ ], an  $R$  of 0.788 has been determined. This value is slightly smaller than 0.807 from chemical data and 0.817 from the equation of Jones (1968).

No linear correlation between  $-\text{sec}(\text{T-O-T})$  and  $\Delta(\text{T-O})$ , the deviation of an individual T-O bond distance from  $\langle \text{T-O} \rangle$ , predicted from Extended Hückel Molecular-Orbital (EHMO) theory and observed by Schlenker et al. (1977) in dehydrated erionite has been observed. Moreover, a check carried out on data of Alberti et al. (1997) confirms that this relationship does not hold for such erionite samples.

Individual T-O-T bond angles are consistent with those reported by Alberti et al. (1997) and Gualtieri et al. (1998), the exception being the anomalous Agate Beach sample showing a T2-O6-T2 angle significantly smaller than the average value of 168(6)°. As expected, differences are observed in dehydrated erionite (Schlenker et al. 1977) due to the partial collapse of the framework.

Despite the very good agreement indices obtained from the refinement, an attempt to detect the presence of offretite stacking faults was carried out following the procedure of Schlenker et al. (1977). However, after a few cycles of refinement the population of the extra Si and O sites required to describe the B'C' ring decreased to zero, providing indication of the absence or very limited presence of stacking faults.

**Extra-framework cations and H<sub>2</sub>O molecules.** The cancrinite cage is filled by K, as reported by Gard and Tait (1973), Alberti et al. (1997), and Gualtieri et al. (1998). Structure refinement indicates an almost complete occupancy of the K1 site. The K atom is 12-fold coordinated by six O2 atoms at 2.926(3) Å and six very distant O3 atoms at 3.367(3) Å. However, the presence of the latter O atoms provides ca. 0.2 valence units (v.u.) to reach a reasonable total of 0.906 v.u., confirming that the inclusion of higher coordination shells is important in the evaluation of the bond valence in the case of alkali cations (Adams 2001).

Significant differences are reported with respect to the crystal structure of Alberti et al. (1997) with respect to the position and site population of the erionite cage. This is most likely due to the presence of significant K to be located within this cage. Three cationic sites and six H<sub>2</sub>O sites (similar to Alberti et al. 1997) have been identified. Ca1 and Ca2 are both approximately located at the same  $z$  coordinate of the corresponding sites reported by Alberti et al. (1997) and Gualtieri et al. (1998) (note the inver-

sion of Ca1 and Ca2 labels in Gualtieri et al. 1998), but they are slightly displaced from the threefold axis. This displacement provides more favorable coordination by the O atoms of both water molecules and framework. Large displacement parameters for both cationic and H<sub>2</sub>O-molecule sites reasonably indicate that the determined positions represent only an average between neighboring split sites, mutually exclusive, occupied by different chemical species in the case of cationic sites, and by different H<sub>2</sub>O-molecule distributions required for correct coordination. Attempts to model such positional disorder using split sites, not imposing constraints on bond distances and angles, failed due to high correlations between the refined parameters. The shortest Ca1-Ca2 contact of 3.314 Å does not imply any constraint on the occupancy of both sites. Further the cationic site labeled as K2 has been observed at special position  $\frac{1}{2}, 0, 0$ . This corresponds to the K site found by Schlenker et al. (1977) in dehydrated erionite and to the Ca4 site found by Gualtieri et al. (1998) in Lady Hill, Shourdo, and Tunguska samples. As indicated in the experimental methods section, Ca3 site scattering (s.s.) decreased immediately to zero during the first refinement cycles. OW11, which is reported by Alberti et al. (1997) to be approximately coplanar with Ca3, shows  $x$  and  $y$  coordinates slightly displaced toward the axis of the cage. Both behaviors could be reasonably explained by the presence of a very small site occupancy at Ca3, impossible to model with the present powder data set. This hypothesis is also supported by the fact that standard deviations of fractional coordinates of OW11 are significantly higher than those of other H<sub>2</sub>O-molecule sites showing a comparable site population.

According to bond-valence analysis (Table 5), Ca1 and Ca2 both offer different possible coordination for different cationic species. In particular, taking into account the mutual exclusion due to very short contacts among H<sub>2</sub>O molecules, Ca1 provides a very favorable distorted sixfold coordination for Mg [Ca1-OW11  $\times 2$  of 2.05(11) Å, Ca1-OW9  $\times 2$  of 2.16(5) Å, and Ca1-OW8  $\times 2$  of 2.37(8) Å] (Fig. 6). Calcium could alternatively receive a possible eightfold coordination, but that is prevented by short OW9-OW10 contacts. Thus, this is the only chemically reasonable location for Mg that is the carrier of a s.s. of 9.6 e<sup>-</sup> compared to the refined value of 13(2). The relevant standard deviations of fractional coordinates, site occupancy, and displacement parameter could result from correlation of parameters. Therefore, we may conclude that Ca1 is filled by Mg. It is worth noting that Mg is exclusively coordinated by water molecules, as found in natural and synthetic zeolites. It should be pointed out that a few short contacts occur within the sixfold coordination, in particular OW8-OW9 of 2.10(2) and OW8-OW11 of 2.15(5) Å. However, this fact can be explained, as previously indicated, considering that the determined positions represent only an average between very close neighboring split, mutually exclusive sites, occupied by different H<sub>2</sub>O molecules.

Ca2, on the contrary, exhibits nine bonding distances with O atoms. However, short contacts prevent the simultaneous presence of OW8 and OW9. Therefore, a possible sevenfold coordination for both Ca and Na [Ca2-OW8 of 2.18(3) Å, Ca2-OW12  $\times 2$  of 2.552(16) Å, Ca2-OW8  $\times 2$  of 2.77(2) Å, Ca2-O5 of 2.922(14) Å, Ca2-OW12 of 3.342(15) Å] may be proposed (Fig. 7). Considering this site as occupied by all available Na and

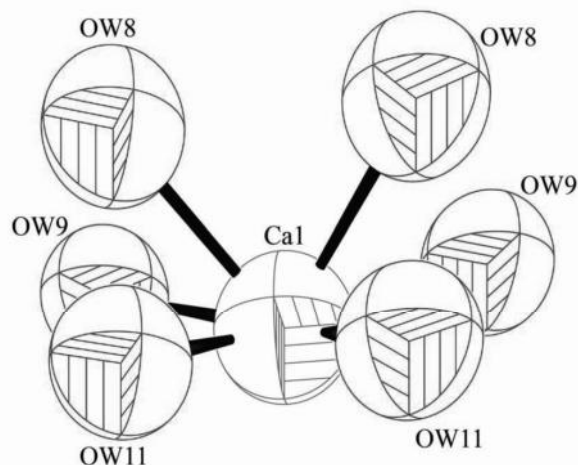


FIGURE 6. ORTEP-3 (Farrugia 1999) plot of the possible coordination around Ca1 site.

Ca (Mn) cations, we obtain a s.s. of  $39.7 e^-$  exactly coincident with the refined value.

The K2 site has been considered as filled by K. This attribution is justified for two reasons. First, apart from very short non-occurring K2-OW12 [ $\times 2$  of  $1.311(13) \text{ \AA}$ ] and K2-OW9 [ $\times 2$  of  $1.97(3) \text{ \AA}$ ] bond distances, it is possible to define a 12-fold coordination (K2-OW10  $\times 2$ , K2-O4  $\times 2$ , K2-O1  $\times 4$ , and K2-OW8  $\times 4$ ) well suited for a K cation. In addition, the refined s.s. is  $15.4(5) e^-$ , as compared to  $16.5 e^-$  considering the presence of the remaining  $0.87$  apfu of K not assigned to the K1 site. This attribution is in agreement with that of Schlenker et al. (1977), who indicated the presence of an internal ion exchange process arising during the dehydration of both erionite and offretite (Mortier et al. 1976), moving the K atom from the center of the  $\epsilon$ -cage to the center of an eight-membered ring.

H<sub>2</sub>O molecules are distributed among six sites. Total refined s.s. for H<sub>2</sub>O molecules corresponds to  $30.5$  water molecules pfu,

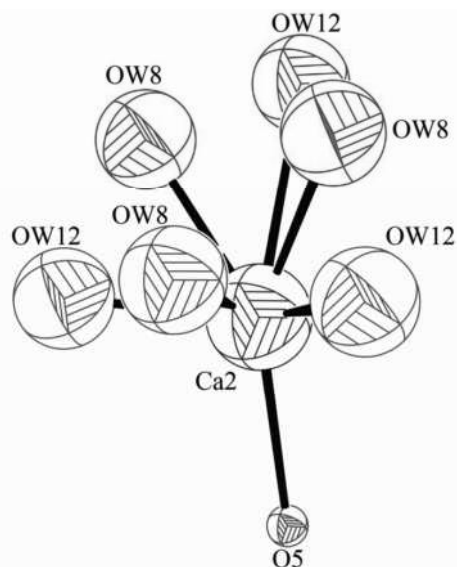


FIGURE 7. ORTEP-3 (Farrugia 1999) plot of the possible coordination around Ca2 site.

a value consistent with literature data (i.e., Coombs et al. 1997; Alberti et al. 1997; Passaglia et al. 1998) but higher than the  $25.7$  H<sub>2</sub>O molecules obtained from thermogravimetric analysis. However, scarcity of material could lead to significant error in the TG analysis. Site population is significantly different with respect to that reported by Alberti et al. (1997), but this clearly reflects the different cationic content of the erionite cage. The most striking difference, apart from site occupancies, is related to the OW8 position, which is significantly displaced along the  $z$  axis. This is required to provide a favorable coordination for Ca1.

Similarly to Alberti et al. (1997), a few OW-OW very short contacts prevent the contemporaneous presence of OW9, OW10, and OW12, as well as OW7 and OW11. It is worth noting that the refined sum of OW7, OW11, OW9, and OW12 occupancies [ $1.11(4)$  and  $1.07(3)$ , respectively] slightly exceeds unity. This can be an effect of correlation between displacement parameters and occupancy as well as, for OW11, that its position and occupancy are not well defined due to the electronic contribution of a neighboring low-occupancy cationic site.

Therefore, we can consider the above OW-OW contacts as never occurring because the sites cannot be simultaneously occupied. To investigate the geometry of the hydrogen bond network possibly occurring, O-O contacts were also identified. Selecting the  $2.5$ – $3.2 \text{ \AA}$  range, as reported by Chiari and Ferraris (1982), OW8, OW11, and OW12 were found to be linked exclusively to H<sub>2</sub>O molecules.

## DISCUSSION

A detailed topochemical model of erionite-K from Rome, Oregon, may be obtained only by fully exploiting the synergy between structural and spectroscopic investigations: on such bases it can be excluded that the observed Fe<sup>3+</sup> is in the zeolite framework in tetrahedrally coordinated sites. On the contrary, it is attributed to octahedrally coordinated cationic sites, though not in extra-framework positions in the erionite cages (i.e., in the structural pores). In fact, the Fe observed from ICP (and reported in reference data) corresponds to ca.  $1.2$  apfu (i.e., to a s.s. of ca.  $30 e^-$ ) and such a quantity could not be accommodated in the erionite structure refinement. In particular, the s.s. of extra-framework sites does not support the presence of Fe, and the sizes of cages could hardly host octahedrally coordinated Fe<sup>3+</sup>-O clusters. Erionite is a microporous material with a three-dimensional intersecting channel system (Fig. 1). All channels are equidimensional with elliptical 8-ring openings of  $0.36 \times 0.51 \text{ nm}$  (Hernandez et al. 2000). The hypothesis of surface Fe, that is, external Fe<sup>3+</sup>-O clusters bound by either weak physisorption or strong chemisorption, must therefore be explored. Attributing this Fe to impurities, the total refined cationic s.s. ( $105.2 e^-$ ) and the s.s. retrieved from recalculated chemical data ( $106.5 e^-$ ) are in very good agreement (Table 4).

The most common iron oxide and hydroxide with Fe<sup>3+</sup> octahedrally coordinated are  $\alpha$ -Fe<sub>2</sub>O<sub>3</sub> (hematite) and  $\alpha$ -FeO(OH) (goethite), respectively. Magnetically ordered materials such as hematite and goethite generally give a six-line (sextet) <sup>57</sup>Fe Mössbauer spectrum, which was not observed in our spectrum. However, in the case of very small particles ( $<10 \text{ nm}$ ) the magnetic sextet collapses into a doublet, and the phenomenon is known as superparamagnetic relaxation (Kündig et al. 1966; Meagher et al.

1988; Bachari et al. 2007). Since the superparamagnetism influence decreases with temperature, another spectrum of erionite was collected at 77 K (Fig. 3b). The low-temperature spectrum is not very different from the RT one and it was modeled by two quadrupole doublets and, tentatively, one magnetic sextet. The IS of all doublets and sextet is about 0.5 mm/s confirming the presence of high-spin Fe<sup>3+</sup> ions. The numerical difference with the RT spectrum is due to an effect known as second-order Doppler shift, which makes the IS increase when temperature decreases. The absorption area of the sextet is very small (5% Fe<sub>tot</sub>) and comparable with the error estimation, thus making its presence questionable, but the magnetic field measured for it is about 54 T, a value typical of hematite. On this basis, two Fe species may be identified: magnetic hematite particles with size ≥10 nm, corresponding to about 5% of total Fe, and superparamagnetic oxide-like nanoparticles with size <10 nm, corresponding to about 95% of total Fe. Due to both the extremely limited particle size and the very low total Fe content, it is now clear why the diffractometric study, though detailed, could not reveal any signal from iron oxide.

The chemical activity of surface Fe oxide nanoparticles in zeolites is known to be very important, and is extensively studied because of catalytic applications (i.e., Bachari et al. 2007; Zecchina et al. 2007). In particular, Bachari et al. (2007) collected a Mössbauer spectrum virtually identical to ours from their synthetic zeolite sample at 77 K. Measuring spectra at extremely low temperature, they were able to further characterize the sizes of their nanoparticles, which clustered around 3 and 9 nm, and concluded that particles of such dimensions may agglomerate on the external surface of silica walls. In our case, the lower constraint is the channel size (<0.5 nm), so that we can reasonably assume that the Fe<sup>3+</sup>-bearing, superparamagnetic, oxide-like nanoparticles are located on the external surface of silica walls and have dimensions between 1 and 9 nm.

#### ACKNOWLEDGMENTS

We acknowledge Aramec Foundation for supporting three weeks of fieldwork, Oriana Strianese for helping sample collections from the study area, Central Microscopy Research Facility of the University of Iowa, for FESEM study, and Turkish National Petroleum Corporation Research Laboratories for the initial work on PXRD study. This work was supported by Università di Roma "La Sapienza" and developed within CNR-IGAG and CNR-IGG research priorities. Thanks are due to G. Cruciani (University of Ferrara) for TGA analysis. We also acknowledge referees, Bice Fubini and three anonymous reviewers, and Aaron Celestian, the associate editor, for their helpful comments and critiques, which improved the manuscript.

#### REFERENCES CITED

- Adams, S. (2001) Relationship between bond valence and bond softness of alkali halides and chalcogenides. *Acta Crystallographica*, B57, 278–287.
- Alberti, A., Martucci, A., Galli, E., and Vezzalini, G. (1997) A reexamination of the crystal structure of erionite. *Zeolites*, 19, 349–352.
- Bachari, K., Millet, J.M.M., Bonville, P., Cherifi, O., and Figueras, F. (2007) Spectroscopic characterization of iron nanoparticles in Fe-mesoporous silicate catalysts. *Journal of Catalysis*, 249, 52–58.
- Bertino, P., Marconi, A., Palumbo, L., Bruni, B.M., Barbone, D., Germano, S., Dogan, A.U., Tassi, G.F., Porta, C., Mutti, L., and Gaudino, G. (2007) Erionite and asbestos differently cause transformation of human mesothelial cells. *International Journal of Cancer*, 121, 2766–2774.
- Brese, N.E. and O'Keefe, M. (1991) Bond-valence parameters for solids. *Acta Crystallographica*, B47, 192–197.
- Bruker AXS (2005) Topas V3: General profile and structure analysis software for powder diffraction data. Bruker AXS, Karlsruhe, Germany.
- Carbone, M., Emri, S., Dogan, A.U., Steele, I., Tuncer, M., Pass, H.I., and Baris, Y.I. (2007) A mesothelioma epidemic in Cappadocia: Scientific developments and unexpected social outcomes. *Nature Review Cancer*, 7, 147–154.
- Carr, A. and Frei, B. (1999) Does vitamin C act as a pro-oxidant under physiological conditions? *The FASEB Journal*, 13, 1007–1023.
- Cheary, R.W. and Coelho, A. (1992) A fundamental parameters approach to X-ray line-profile fitting. *Journal of Applied Crystallography*, 25, 109–121.
- Chiari, G. and Ferraris, G. (1982) The water molecule in crystalline hydrates studied by neutron diffraction. *Acta Crystallographica*, B38, 2331–2341.
- Coombs, D.C., Alberti, A., Armbruster, T., Artioli, G., Colella, C., Galli, E., Grice, J.D., Liebau, F., Mandarino, J.A., Minato, H., Nickel, E.H., Passaglia, E., Peacor, D.R., Quartieri, S., Rinaldi, R., Ross, M., Sheppard, R.A., Tillmanns, E., and Vezzalini, G. (1997) Recommended nomenclature for zeolite minerals: Report of the subcommittee of the International Mineralogical Association, Commission on New Minerals and Mineral Names. *Canadian Mineralogist*, 35, 1571–1606.
- Dogan, A.U. and Dogan, M. (2008) Re-evaluation and re-classification of erionite series minerals. *Environmental Geochemistry and Health*, 30, 355–366.
- Dogan, A.U., Baris, Y.I., Dogan, M., Emri, S., Steele, I., Elmishad, A.G., and Carbone, M. (2006) Genetic predisposition to fiber carcinogenesis causes a mesothelioma epidemic in Turkey. *Cancer Research*, 66, 5063–5068.
- Dogan, A.U., Dogan, M., and Hoskins, J.A. (2008) Erionite series minerals: Mineralogical and carcinogenic properties. *Environmental Geochemistry and Health*, 30, 367–381.
- Dowty, E. (2000) ATOMS for Windows. Shape Software, Kingsport, Tennessee.
- Eberly Jr., P.E. (1964) Adsorption properties of naturally occurring erionite and its cationic-exchanged forms. *American Mineralogist*, 49, 30–40.
- Eborn, S.K. and Aust, A.E. (1995) Effect of iron acquisition on induction of DNA single-strand breaks by erionite, a carcinogenic mineral fiber. *Archives of Biochemistry and Biophysics*, 316, 507–514.
- Fach, E., Kristovich, R., Long, J.F., Waldman, W.J., Dutta, P.K., and Williams, M.V. (2003) The effect of iron on the biological activities of erionite and mordenite. *Environment International*, 29, 451–458.
- Farrugia, L.J. (1999) ORTEP-3 for Windows. University of Glasgow, Scotland.
- Finger, L.W., Cox, D.E., and Jephcoat, A.P. (1994) A correction for powder diffraction peak asymmetry due to axial divergence. *Journal of Applied Crystallography*, 27, 892–900.
- Fubini, B. and Otero Aréan, C. (1999) Chemical aspects of the toxicity of inhaled mineral dusts. *Chemical Society Reviews*, 28, 373–381.
- Gard, J.A. and Tait, J.M. (1973) Refinement of the crystal structure of erionite. *Proceedings of the 3<sup>rd</sup> International Conference on Molecular Sieves*, p. 94–99. University Press, Leuven.
- Gottardi, G. and Galli, E. (1985) *Natural Zeolites*. Springer-Verlag, Heidelberg.
- Gualtieri, A., Artioli, G., Passaglia, E., Bigi, S., Viani, A., and Hanson, J.C. (1998) Crystal structure-crystal chemistry relationships in the zeolites erionite and offretite. *American Mineralogist*, 83, 590–600.
- Hernandez, M.A., Corona, L., and Rojas, F. (2000) Adsorption characteristics of natural erionite, clinoptilolite and mordenite zeolites from Mexico. *Adsorption*, 6, 33–45.
- Jones, J.B. (1968) Al-O and Si-O tetrahedral distances in aluminosilicate framework structures. *Acta Crystallographica*, B24, 355–358.
- Kamp, D.W. and Weitzman, S.A. (1999) The molecular basis of asbestos induced lung injury. *Thorax*, 54, 638–652.
- Kane, A.B., Boffetta, P., Saracci, R., and Wilbourn, J.D. (1996) *Mechanisms of Fibre Carcinogenesis*, 157 p. IARC Scientific Publication 140, Lyon, France.
- Kawahara, A. and Curien, H. (1969) La structure cristalline de l'érionite. *Bulletin de la Société Française de Minéralogie et de Cristallographie*, 92, 250–256.
- Kündig, W., Bömmel, H., Constabaris, G., and Lindquist, R.H. (1966) Some properties of supported small  $\alpha$ -Fe<sub>2</sub>O<sub>3</sub> particles determined with the Mössbauer effect. *Physical Review*, 142, 327–333.
- Lagarec, K. and Rancourt, D.G. (1998) RECOIL. Mössbauer spectral analysis software for Windows, version 1.0. Department of Physics, University of Ottawa, Canada.
- Larson, A.C. and Von Dreele, R.B. (1985) General structure analysis system (GSAS). Los Alamos National Laboratory Report LAUR 86-748.
- Long, G.J., Cranshaw, T.E., and Longworth, G. (1983) The ideal Mössbauer effect absorber thickness. *Mössbauer Effect Reference Data Journal*, 6, 42–49.
- Meagher, A., Nair, V., and Szostak, R. (1988) A Mössbauer study of ZSM-5-type ferrisilicates. *Zeolites*, 8, 3–11.
- Mortier, W.J., Pluth, J.J., and Smith, J.V. (1976) The crystal structure of dehydrated offretite with stacking faults of erionite type. *Zeitschrift für Kristallographie*, 143, 319–322.
- Passaglia, E., Artioli, G., and Gualtieri, A. (1998) Crystal chemistry of the zeolites erionite and offretite. *American Mineralogist*, 83, 577–589.
- Rancourt, D.G. (1994a) Mössbauer spectroscopy of minerals. I. Inadequacy of Lorentzian-line doublets in fitting spectra arising from quadrupole splitting distributions. *Physics and Chemistry of Minerals*, 21, 244–249.
- (1994b) Mössbauer spectroscopy of minerals. II. Problem of resolving *cis* and *trans* octahedral Fe<sup>2+</sup> sites. *Physics and Chemistry of Minerals*, 21, 250–257.
- Rancourt, D.G. and Ping, J.Y. (1991) Voigt-based methods for arbitrary-shape

- static hyperfine parameter distributions in Mössbauer spectroscopy. *Nuclear Instruments and Methods in Physics Research*, B58, 85–97.
- Robledo, R. and Mossman, R. (1999) Cellular and molecular mechanisms of asbestos-induced fibrosis. *Journal of Cellular Physiology*, 180, 158–166.
- Ruda, T.A. and Dutta, P.K. (2005) Fenton Chemistry of Fe<sup>III</sup>-exchanged zeolitic minerals treated with antioxidants. *Environmental Science and Technology*, 39, 6147–6152.
- Schlenker, J.L., Pluth, J.J., and Smith, J.V. (1977) Dehydrated natural erionite with stacking faults of the offretite type. *Acta Crystallographica*, B33, 3265–3268.
- Staples, L.W. and Gard, J.A. (1959) The fibrous zeolite erionite: Its occurrence, unit cell, and structure. *Mineralogical Magazine*, 32, 261–281.
- Thompson, P., Cox, D.E., and Hastings, J.B. (1987) Rietveld refinement of Debye-Scherrer synchrotron X-ray data from Al<sub>2</sub>O<sub>3</sub>. *Journal of Applied Crystallography*, 20, 79–83.
- Toby, B.H. (2001) EXPGUI, a graphical user interface for GSAS. *Journal of Applied Crystallography*, 34, 210–213.
- Von Dreele, R.B. (1997) Quantitative texture analysis by Rietveld refinement. *Journal of Applied Crystallography*, 30, 517–525.
- Young, R.A. (1993) Introduction to the Rietveld method. In R.A. Young, Ed., *The Rietveld Method*, p. 1–38. Oxford Science, U.K.
- Zecchina, A., Rivallan, M., Berlier, G., Lamberti, C., and Ricchiardi, G. (2007) Structure and nuclearity of active sites in Fe-zeolites: Comparison with iron sites in enzymes and homogeneous catalysts. *Physical Chemistry Chemical Physics*, 9, 3483–3499.

MANUSCRIPT RECEIVED DECEMBER 3, 2008

MANUSCRIPT ACCEPTED APRIL 27, 2009

MANUSCRIPT HANDLED BY AARON CELESTIAN